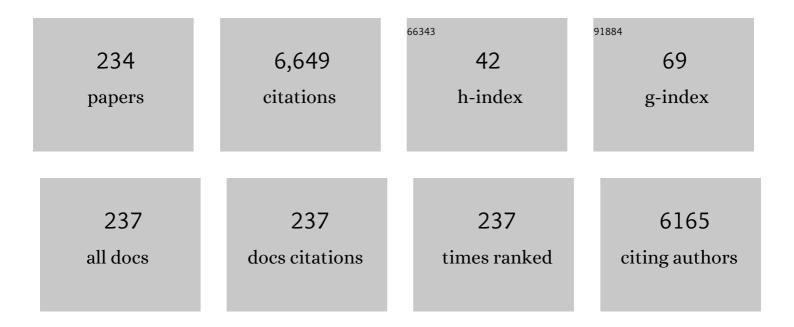
Yicheng Ni

List of Publications by Year in descending order

Source: https://exaly.com/author-pdf/6488660/publications.pdf Version: 2024-02-01



YICHENC NI

#	Article	IF	CITATIONS
1	Local Recurrence After Hepatic Radiofrequency Coagulation. Annals of Surgery, 2005, 242, 158-171.	4.2	634
2	Effect of Vascular Targeting Agent in Rat Tumor Model: Dynamic Contrast-enhanced versus Diffusion-weighted MR Imaging. Radiology, 2005, 237, 492-499.	7.3	158
3	Diffusion-weighted MR Imaging in Monitoring the Effect of a Vascular Targeting Agent on Rhabdomyosarcoma in Rats. Radiology, 2005, 234, 756-764.	7.3	147
4	Radiofrequency Ablation versus Resection for Resectable Colorectal Liver Metastases: Time for a Randomized Trial?. Digestive Surgery, 2008, 25, 445-460.	1.2	140
5	Radiofrequency Ablation Versus Resection for Resectable Colorectal Liver Metastases: Time for a Randomized Trial?. Annals of Surgical Oncology, 2008, 15, 144-157.	1.5	138
6	Automated quantitative gait analysis in animal models of movement disorders. BMC Neuroscience, 2010, 11, 92.	1.9	130
7	Radiofrequency Ablation for Eradication of Pulmonary Tumor in Rabbits. Journal of Surgical Research, 2001, 99, 265-271.	1.6	127
8	Toward Highly Potent Cancer Agents by Modulating the C-2 Group of the Arylthioindole Class of Tubulin Polymerization Inhibitors. Journal of Medicinal Chemistry, 2013, 56, 123-149.	6.4	107
9	Antihyperglycemic, antihyperlipidemic and antioxidant effects of ethanol and aqueous extracts of Cyclocarya paliurus leaves in type 2 diabetic rats. Journal of Ethnopharmacology, 2013, 150, 1119-1127.	4.1	106
10	Evans Blue Dye: A Revisit of Its Applications in Biomedicine. Contrast Media and Molecular Imaging, 2018, 2018, 1-10.	0.8	104
11	Ex VivoExperiment on Radiofrequency Liver Ablation with Saline Infusion through a Screw-Tip Cannulated Electrode. Journal of Surgical Research, 1997, 71, 19-24.	1.6	103
12	In vitro labeling and MRI of mesenchymal stem cells from human umbilical cord blood. Magnetic Resonance Imaging, 2006, 24, 611-617.	1.8	88
13	Noninvasive Measurements of Infarct Size After Thrombolysis With a Necrosis-Avid MRI Contrast Agent. Circulation, 1999, 99, 690-696.	1.6	87
14	US-guided Percutaneous Microwave Coagulation of Small Breast Cancers: A Clinical Study. Radiology, 2012, 263, 364-373.	7.3	85
15	Necrosis Avid Contrast Agents. Investigative Radiology, 2005, 40, 526-535.	6.2	82
16	A Dual-targeting Anticancer Approach: Soil and Seed Principle. Radiology, 2011, 260, 799-807.	7.3	81
17	A Comparative Study on Validation of a Novel Cooled-Wet Electrode for Radiofrequency Liver Ablation. Investigative Radiology, 2000, 35, 438-444.	6.2	81
18	An ex vivo study on radiofrequency tissue ablation: increased lesion size by using an "expandable-wet" electrode. European Radiology, 2001, 11, 1841-1847.	4.5	77

#	Article	IF	CITATIONS
19	Localization of metalloporphyrin-induced "specific―enhancement in experimental liver tumors: Comparison of magnetic resonance imaging, microangiographic, and histologic findings. Academic Radiology, 1995, 2, 687-699.	2.5	76
20	First preclinical evaluation of mono-[123I]iodohypericin as a necrosis-avid tracer agent. European Journal of Nuclear Medicine and Molecular Imaging, 2006, 33, 595-601.	6.4	76
21	Metalloporphyrins and Functional Analogues as MRI Contrast Agents. Current Medical Imaging, 2008, 4, 96-112.	0.8	71
22	Antihyperlipidemic effect of Cyclocarya paliurus (Batal.) Iljinskaja extract and inhibition of apolipoprotein B48 overproduction in hyperlipidemic mice. Journal of Ethnopharmacology, 2015, 166, 286-296.	4.1	71
23	Non-invasive detection and quantification of acute myocardial infarction in rabbits using mono-[1231]iodohypericin ÂSPECT. European Heart Journal, 2007, 29, 260-269.	2.2	68
24	Diffusion-Weighted Magnetic Resonance Imaging Allows Noninvasive In Vivo Monitoring of the Effects of Combretastatin A-4 Phosphate after Repeated Administration. Neoplasia, 2005, 7, 779-787.	5.3	67
25	Mammalian models of chemically induced primary malignancies exploitable for imaging-based preclinical theragnostic research. Quantitative Imaging in Medicine and Surgery, 2015, 5, 708-29.	2.0	67
26	Prognostic significance of 18FDG PET/CT in colorectal cancer patients with liver metastases: a meta-analysis. Cancer Imaging, 2015, 15, 19.	2.8	64
27	Magnetic Resonance Imaging-Histomorphologic Correlation Studies on Paramagnetic Metalloporphyrins in Rat Models of Necrosis. Investigative Radiology, 1997, 32, 770-779.	6.2	64
28	Prolonged positive contrast enhancement with Gdâ€EOBâ€DTPA in experimental liver tumors: Potential value in tissue characterization. Journal of Magnetic Resonance Imaging, 1994, 4, 355-363.	3.4	63
29	Experimental and Clinical Radiofrequency Ablation: Proposal for Standardized Description of Coagulation Size and Geometry. Annals of Surgical Oncology, 2007, 14, 1381-1396.	1.5	62
30	A review on various targeted anticancer therapies. Targeted Oncology, 2012, 7, 69-85.	3.6	62
31	Treatment of Rodent Liver Tumor With Combretastatin A4 Phosphate. Investigative Radiology, 2009, 44, 44-53.	6.2	58
32	In Vivo MR Tracking of Mesenchymal Stem Cells in Rat Liver after Intrasplenic Transplantation. Radiology, 2007, 245, 206-215.	7.3	57
33	Value of T2-Weighted Magnetic Resonance Imaging Early After Myocardial Infarction in Dogs. Investigative Radiology, 2002, 37, 77-85.	6.2	54
34	Electrodes and multiple electrode systems for radiofrequency ablation: a proposal for updated terminology. European Radiology, 2005, 15, 798-808.	4.5	54
35	A Review on Curability of Cancers: More Efforts for Novel Therapeutic Options Are Needed. Cancers, 2019, 11, 1782.	3.7	53
36	Relationship Between ¹⁸ F-FDG Accumulation and Lactate Dehydrogenase A Expression in Lung Adenocarcinomas. Journal of Nuclear Medicine, 2014, 55, 1766-1771.	5.0	50

#	Article	IF	CITATIONS
37	Sequential Systemic Administrations of Combretastatin A4 Phosphate and Radioiodinated Hypericin Exert Synergistic Targeted Theranostic Effects with Prolonged Survival on SCID Mice Carrying Bifocal Tumor Xenografts. Theranostics, 2013, 3, 127-137.	10.0	48
38	Cyclocarya paliurus extract modulates adipokine expression and improves insulin sensitivity by inhibition of inflammation in mice. Journal of Ethnopharmacology, 2014, 153, 344-351.	4.1	48
39	<i>Cyclocarya paliurus</i> prevents high fat diet induced hyperlipidemia and obesity in Sprague–Dawley rats. Canadian Journal of Physiology and Pharmacology, 2015, 93, 677-686.	1.4	48
40	Synthesis, Characterization, and Pharmacokinetic Evaluation of a Potential MRI Contrast Agent Containing Two Paramagnetic Centers with Albumin Binding Affinity. Chemistry - A European Journal, 2005, 11, 3077-3086.	3.3	47
41	Rodent stroke induced by photochemical occlusion of proximal middle cerebral artery: Evolution monitored with MR imaging and histopathology. European Journal of Radiology, 2007, 63, 68-75.	2.6	45
42	Small-Animal PET of Tumor Damage Induced by Photothermal Ablation with 64Cu-Bis-DOTA-Hypericin. Journal of Nuclear Medicine, 2011, 52, 792-799.	5.0	44
43	Exploring Theranostic Potentials of Radioiodinated Hypericin in Rodent Necrosis Models. Theranostics, 2012, 2, 1010-1019.	10.0	44
44	Radiofrequency Ablation for Eradication of Renal Tumor in a Rabbit Model by Using a Cooled-tip Electrode Technique. Annals of Surgical Oncology, 2001, 8, 651-657.	1.5	43
45	Inhibited atherosclerotic plaque formation by local administration of magnetically labeled endothelial progenitor cells (EPCs) in a rabbit model. Atherosclerosis, 2009, 205, 80-86.	0.8	43
46	Paramagnetic metalloporphyrins: From enhancers of malignant tumors to markers of myocardial infarcts. Academic Radiology, 1996, 3, S395-S397.	2.5	42
47	Radiolabeled iodohypericin as tumor necrosis avid tracer: diagnostic and therapeutic potential. International Journal of Cancer, 2012, 131, E129-37.	5.1	42
48	Hypericin as a Marker for Determination of Tissue Viability After Intratumoral Ethanol Injection in a Murine Liver Tumor Model. Academic Radiology, 2008, 15, 107-113.	2.5	41
49	Tumor resistance to vascular disrupting agents: mechanisms, imaging, and solutions. Oncotarget, 2016, 7, 15444-15459.	1.8	41
50	The Uptake of Manganese Dipyridoxal-Diphosphate by Chemically Induced Hepatocellular Carcinoma in Rats; A Correlation between Contrast-Media-Enhanced Magnetic Resonance Imaging, Tumor Differentiation, and Vascularization. Investigative Radiology, 1993, 28, 520-527.	6.2	39
51	Magnetic resonance imaging after radiofrequency ablation in a rodent model of liver tumor: tissue characterization using a novel necrosis-avid contrast agent. European Radiology, 2006, 16, 1031-1040.	4.5	39
52	Pharmacokinetic andin vivo evaluation of a self-assembled gadolinium(III)-iron(II) contrast agent with high relaxivity. Contrast Media and Molecular Imaging, 2006, 1, 267-278.	0.8	39
53	Liver Tumor Model with Implanted Rhabdomyosarcoma in Rats: MR Imaging, Microangiography, and Histopathologic Analysis. Radiology, 2006, 239, 554-562.	7.3	39
54	Magnetic Resonance Imaging, Microangiography, and Histology in a Rat Model of Primary Liver Cancer. Investigative Radiology, 1992, 27, 689-697.	6.2	38

#	Article	IF	CITATIONS
55	Preliminary in vivo evaluation of a novel 99mTc-Labeled HYNIC-cys-annexin A5 as an apoptosis imaging agent. Bioorganic and Medicinal Chemistry Letters, 2008, 18, 3794-3798.	2.2	38
56	Mn-DPDP Enhanced MRI in Experimental Bile Duct Obstruction. Journal of Computer Assisted Tomography, 1993, 17, 290-296.	0.9	35
57	Microplasmin Reduces Ischemic Brain Damage and Improves Neurological Function in a Rat Stroke Model Monitored With MRI. Stroke, 2004, 35, 2402-2406.	2.0	35
58	Tumor models and specific contrast agents for small animal imaging in oncology. Methods, 2009, 48, 125-138.	3.8	35
59	MRI Contrast Enhancement of Necrosis by MP-2269 and Gadophrin-2 in a Rat Model of Liver Infarction. Investigative Radiology, 2001, 36, 97-103.	6.2	34
60	Morphological, functional and metabolic imaging biomarkers: assessment of vascular-disrupting effect on rodent liver tumours. European Radiology, 2010, 20, 2013-2026.	4.5	34
61	Evaluation of Hypericin: Effect of Aggregation on Targeting Biodistribution. Journal of Pharmaceutical Sciences, 2015, 104, 215-222.	3.3	34
62	In Vivo Differentiation of Magnetically Labeled Mesenchymal Stem Cells Into Hepatocytes for Cell Therapy to Repair Damaged Liver. Investigative Radiology, 2010, 45, 625-633.	6.2	33
63	InÂvivo hepatocyte MR imaging using lactose functionalized magnetoliposomes. Biomaterials, 2014, 35, 1015-1024.	11.4	32
64	Diffusion weighted imaging in small rodents using clinical MRI scanners. Methods, 2007, 43, 12-20.	3.8	30
65	Quantification of liver fat in mice: comparing dual-echo Dixon imaging, chemical shift imaging, and 1H-MR spectroscopy. Journal of Lipid Research, 2011, 52, 1847-1855.	4.2	30
66	Visualization of Stroke with Clinical MR Imagers in Rats: A Feasibility Study. Radiology, 2004, 233, 905-911.	7.3	29
67	Diffusionâ€weighted MRI of hepatic tumor in rats: Comparison between in vivo and postmortem imaging acquisitions. Journal of Magnetic Resonance Imaging, 2009, 29, 621-628.	3.4	29
68	Utilisation of Chick Embryo Chorioallantoic Membrane as a Model Platform for Imaging-Navigated Biomedical Research. Cells, 2021, 10, 463.	4.1	29
69	Necrosis Avidity: A Newly Discovered Feature of Hypericin and its Preclinical Applications in Necrosis Imaging. Theranostics, 2013, 3, 667-676.	10.0	28
70	Hypericin as a marker for determination of tissue viability after radiofrequency ablation in a murine liver tumor model. Oncology Reports, 2008, 19, 927-32.	2.6	28
71	A modified rabbit model of reperfused myocardial infarction for cardiac MR imaging research. International Journal of Cardiovascular Imaging, 2009, 25, 289-298.	1.5	27
72	Topical HDL administration reduces vein graft atherosclerosis in apo E deficient mice. Atherosclerosis, 2011, 214, 271-278.	0.8	27

#	Article	IF	CITATIONS
73	Pharmacologic Effects of Cannabidiol on Acute Reperfused Myocardial Infarction in Rabbits. Journal of Cardiovascular Pharmacology, 2015, 66, 354-363.	1.9	27
74	Discovery of Radioiodinated Monomeric Anthraquinones as a Novel Class of Necrosis Avid Agents for Early Imaging of Necrotic Myocardium. Scientific Reports, 2016, 6, 21341.	3.3	26
75	Enhanced Magnetic Resonance Imaging for Tissue Characterization of Liver Abnormalities with Hepatobiliary Contrast Agents. Topics in Magnetic Resonance Imaging, 1998, 9, 183.	1.2	25
76	Necrosis-Avid Contrast Agents. Academic Radiology, 2002, 9, S98-S101.	2.5	25
77	Development and evaluation of a 68Ga labeled pamoic acid derivative for in vivo visualization of necrosis using positron emission tomography. Bioorganic and Medicinal Chemistry, 2010, 18, 5274-5281.	3.0	25
78	Potential role of bile duct collaterals in the recovery of the biliary obstruction: Experimental study in rats using microcholangiography, histology, serology and magnetic resonance imaging. Hepatology, 1994, 20, 1557-1566.	7.3	24
79	Necrosis Avidity of ^{99m} Tc(CO) ₃ -Labeled Pamoic acid Derivatives: Synthesis and Preliminary Biological Evaluation in Animal Models of Necrosis. Bioconjugate Chemistry, 2007, 18, 1924-1934.	3.6	24
80	Synthesis and preliminary evaluation of mono-[1231]iodohypericin monocarboxylic acid as a necrosis avid imaging agent. Bioorganic and Medicinal Chemistry Letters, 2007, 17, 4001-4005.	2.2	24
81	Localization and determination of infarct size by Gd-Mesoporphyrin enhanced MRI in dogs. International Journal of Cardiovascular Imaging, 1997, 13, 499-507.	0.6	23
82	Evaluation of tumor affinity of mono-[1231]iodohypericin and mono-[1231]iodoprotohypericin in a mouse model with a RIF-1 tumor. Contrast Media and Molecular Imaging, 2007, 2, 113-119.	0.8	23
83	Detection and quantification of acute reperfused myocardial infarction in rabbits using DISA-SPECT/CT and 3.0T cardiac MRI. International Journal of Cardiology, 2013, 168, 4191-4198.	1.7	23
84	Radiolabeled Rhein as Small-Molecule Necrosis Avid Agents for Imaging of Necrotic Myocardium. Analytical Chemistry, 2017, 89, 1260-1266.	6.5	23
85	Implications of Web of Science journal impact factor for scientific output evaluation in 16 institutions and investigators' opinion. Quantitative Imaging in Medicine and Surgery, 2014, 4, 453-61.	2.0	23
86	Exploration of the mechanism underlying the tumor necrosis avidity of hypericin. Oncology Reports, 2008, 19, 921-6.	2.6	23
87	Murine liver implantation of radiation-induced fibrosarcoma: characterization with MR imaging, microangiography and histopathology. European Radiology, 2008, 18, 1422-1430.	4.5	22
88	Expression profiling of long noncoding RNAs associated with vasculogenic mimicry in osteosarcoma. Journal of Cellular Biochemistry, 2019, 120, 12473-12488.	2.6	22
89	Necrosis targeted radiotherapy with iodine-131-labeled hypericin to improve anticancer efficacy of vascular disrupting treatment in rabbit VX2 tumor models. Oncotarget, 2015, 6, 14247-14259.	1.8	22
90	Bipolar radiofrequency ablation with four electrodes: Ex vivo liver experiments and finite element method analysis. Influence of inter-electrode distance on coagulation size and geometry. International Journal of Hyperthermia, 2012, 28, 686-697.	2.5	21

#	Article	IF	CITATIONS
91	A Novel In Vivo Rabbit Model of Abdominal Aortic Aneurysm Induced by Periarterial Incubation of Papain. Journal of Vascular and Interventional Radiology, 2012, 23, 1529-1536.	0.5	21
92	Necrosis-targeted combinational theragnostic approach to treat cancer. Oncotarget, 2014, 5, 2934-2946.	1.8	21
93	Bipolar radiofrequency ablation with 2 × 2 electrodes as a building block for matrix radiofrequency ablation: <i>Ex vivo</i> liver experiments and finite element method modelling. International Journal of Hyperthermia, 2015, 31, 649-665.	2.5	20
94	Necrosis affinity evaluation of ¹³¹ I-hypericin in a rat model of induced necrosis. Journal of Drug Targeting, 2013, 21, 604-610.	4.4	19
95	Radioiodinated Hypericin: Its Biodistribution, Necrosis Avidity and Therapeutic Efficacy are Influenced by Formulation. Pharmaceutical Research, 2014, 31, 278-290.	3.5	19
96	Synthesis and Preclinical Evaluation of Radioiodinated Hypericin Dicarboxylic Acid as a Necrosis Avid Agent in Rat Models of Induced Hepatic, Muscular, and Myocardial Necroses. Molecular Pharmaceutics, 2016, 13, 232-240.	4.6	19
97	Updated developments on molecular imaging and therapeutic strategies directed against necrosis. Acta Pharmaceutica Sinica B, 2019, 9, 455-468.	12.0	19
98	Evaluation of radiofrequency ablation as an alternative for the treatment of brain tumor in rabbits. Journal of Neuro-Oncology, 2002, 56, 119-126.	2.9	18
99	Rat cerebral ischemia induced with photochemical occlusion of proximal middle cerebral artery: a stroke model for MR imaging research. Magnetic Resonance Materials in Physics, Biology, and Medicine, 2004, 17, 103-108.	2.0	18
100	Diverse Responses to Vascular Disrupting Agent Combretastatin A4 Phosphate: A Comparative Study in Rats with Hepatic and Subcutaneous Tumor Allografts Using MRI Biomarkers, Microangiography, and Histopathology. Translational Oncology, 2013, 6, 42-50.	3.7	18
101	Evaluation of cardiac arrhythmic risks using a rabbit model of left ventricular systolic dysfunction. European Journal of Pharmacology, 2018, 832, 145-155.	3.5	18
102	Power Doppler ultrasound and contrast-enhanced ultrasound demonstrate non-invasive tumour vascular response to anti-vascular therapy in canine cancer patients. Scientific Reports, 2019, 9, 9262.	3.3	18
103	Exploring Multifunctional Features of Necrosis Avid Contrast Agents. Academic Radiology, 2002, 9, S488-S490.	2.5	17
104	Dynamic susceptibility contrast-enhanced perfusion MR imaging at 1.5 T predicts final infarct size in a rat stroke model. Journal of Neuroscience Methods, 2005, 141, 55-60.	2.5	17
105	Microplasmin and Tissue Plasminogen Activator: Comparison of Therapeutic Effects in Rat Stroke Model at Multiparametric MR Imaging. Radiology, 2007, 244, 429-438.	7.3	17
106	Magnetic Resonance Imaging of Acute Reperfused Myocardial Infarction: Intraindividual Comparison of ECIII-60 and Gd-DTPA in a Swine Model. CardioVascular and Interventional Radiology, 2007, 30, 248-256.	2.0	17
107	Comparative Study of Iodine-123-Labeled Hypericin and 99mTc-Labeled Hexakis [2-Methoxy Isobutyl Isonitrile] in a Rabbit Model of Myocardial Infarction. Journal of Cardiovascular Pharmacology, 2013, 62, 304-311.	1.9	17
108	The first study on therapeutic efficacies of a vascular disrupting agent CA4P among primary hepatocellular carcinomas with a full spectrum of differentiation and vascularity: Correlation of MRIâ€microangiographyâ€histopathology in rats. International Journal of Cancer, 2018, 143, 1817-1828.	5.1	17

#	Article	IF	CITATIONS
109	Multiparametric MRI biomarkers for measuring vascular disrupting effect on cancer. World Journal of Radiology, 2011, 3, 1.	1.1	17
110	Small Molecule Sequential Dual-Targeting Theragnostic Strategy (SMSDTTS): from Preclinical Experiments towards Possible Clinical Anticancer Applications. Journal of Cancer, 2013, 4, 133-145.	2.5	16
111	Hypericin as a Marker for Determination of Myocardial Viability in a Rat Model of Myocardial Infarction. Photochemistry and Photobiology, 2014, 90, 867-872.	2.5	16
112	Comparison of iron oxide particles (AMI 227) with a gadolinium complex (Gd-DOTA) in dynamic susceptibility contrast MR imagings (FLASH and EPI) for both phantom and rat brain at 1.5 tesla. Journal of Magnetic Resonance Imaging, 1999, 9, 447-453.	3.4	15
113	A rabbit model of atherosclerosis at carotid artery: MRI visualization and histopathological characterization. European Radiology, 2008, 18, 2174-2181.	4.5	15
114	Formulation of 3D finite elements for hepatic radiofrequency ablation. International Journal of Modelling, Identification and Control, 2010, 9, 225.	0.2	15
115	Diffusion-weighted MR imaging allows monitoring the effect of combretastatin A4 phosphate on rabbit implanted VX2 tumor model: 12-Day dynamic results. European Journal of Radiology, 2012, 81, 578-583.	2.6	15
116	Enhanced Antitumor Efficacy of a Vascular Disrupting Agent Combined with an Antiangiogenic in a Rat Liver Tumor Model Evaluated by Multiparametric MRI. PLoS ONE, 2012, 7, e41140.	2.5	15
117	Improvement of solubility and targetability of radioiodinated hypericin by using sodium cholate based solvent in rat models of necrosis. Journal of Drug Targeting, 2014, 22, 304-312.	4.4	15
118	Imaging Cell Death: Focus on Early Evaluation of Tumor Response to Therapy. Bioconjugate Chemistry, 2020, 31, 1025-1051.	3.6	15
119	Dynamic Contrast-Enhanced and Diffusion-Weighted Magnetic Resonance Imaging Noninvasive Evaluation of Vascular Disrupting Treatment on Rabbit Liver Tumors. PLoS ONE, 2013, 8, e82649.	2.5	15
120	Detection and characterization of primary liver cancer in rats by MSâ€264â€enhanced MRI. Magnetic Resonance in Medicine, 1996, 35, 532-539.	3.0	14
121	Occlusive Myocardial Infarction Enhanced or Not Enhanced with Necrosis-avid Contrast Agents at MR Imaging. Radiology, 2002, 225, 603-606.	7.3	14
122	Delayed perfusion phenomenon in a rat stroke model at 1.5T MR: An imaging sign parallel to spontaneous reperfusion and ischemic penumbra?. European Journal of Radiology, 2007, 61, 70-78.	2.6	14
123	Preclinical Imaging of Therapy Response Using Metabolic and Apoptosis Molecular Imaging. Molecular Imaging and Biology, 2011, 13, 995-1002.	2.6	14
124	Pretargeting of necrotic tumors with biotinylated hypericin using 123I-labeled avidin: evaluation of a two-step strategy. Investigational New Drugs, 2012, 30, 2132-2140.	2.6	14
125	Radiopharmaceutical evaluation of ¹³¹ I-protohypericin as a necrosis avid compound. Journal of Drug Targeting, 2015, 23, 417-426.	4.4	14
126	Radiopharmaceutical study on Iodine-131-labelled hypericin in a canine model of hepatic RFA-induced coagulative necrosis. Radiologia Medica, 2015, 120, 213-221.	7.7	14

#	Article	IF	CITATIONS
127	Characterization of a rat orthotopic pancreatic head tumor model using threeâ€dimensional and quantitative multiâ€parametric MRI. NMR in Biomedicine, 2017, 30, e3676.	2.8	14
128	Synthesis and Biological Evaluation of Rhein-Based MRI Contrast Agents for in Vivo Visualization of Necrosis. Analytical Chemistry, 2018, 90, 13249-13256.	6.5	14
129	Combining combretastatin A4 phosphate with ginsenoside Rd synergistically inhibited hepatocellular carcinoma by reducing HIF-1α via PI3K/AKT/mTOR signalling pathway. Journal of Pharmacy and Pharmacology, 2021, 73, 263-271.	2.4	14
130	Hypericin as a marker for determination of tissue viability after radiofrequency ablation in a murine liver tumor model. Oncology Reports, 2008, , .	2.6	13
131	Influence of the vascular damaging agents DMXAA and ZD6126 on hypericin distribution and accumulation in RIF-1 tumors. Journal of Cancer Research and Clinical Oncology, 2011, 137, 1619-1627.	2.5	13
132	Towards Stratifying Ischemic Components by Cardiac MRI and Multifunctional Stainings in a Rabbit Model of Myocardial Infarction. Theranostics, 2014, 4, 24-35.	10.0	13
133	Combretastatin A4 phosphate treatment induces vasculogenic mimicry formation of W256 breast carcinoma tumor in vitro and in vivo. Tumor Biology, 2015, 36, 8499-8510.	1.8	13
134	Rheumotologitsts' view on the use of hydroxychloroquine to treat COVID-19. Emerging Microbes and Infections, 2020, 9, 830-832.	6.5	13
135	Lipomatous metaplasia identified in rabbits with reperfused myocardial infarction by 3.0ÂT magnetic resonance imaging and histopathology. BMC Medical Imaging, 2013, 13, 18.	2.7	12
136	Sodium cholate, a solubilizing agent for the necrosis avid radioiodinated hypericin in rabbits with acute myocardial infarction. Drug Delivery, 2015, 22, 427-435.	5.7	12
137	Migration-inducing gene-7 independently predicts poor prognosis of human osteosarcoma and is associated with vasculogenic mimicry. Experimental Cell Research, 2018, 369, 80-89.	2.6	12
138	Tumor necrosis targeted radiotherapy of non-small cell lung cancer using radioiodinated protohypericin in a mouse model. Oncotarget, 2015, 6, 26400-26410.	1.8	12
139	Necrosis Avidity of Organic Compounds: A Natural Phenomenon with Exploitable Theragnostic Potentials. Current Medicinal Chemistry, 2015, 22, 1829-1849.	2.4	12
140	Comparison Between Nonspecific and Necrosis-avid Gadolinium Contrast Agents in Vascular Disrupting Agent-Induced Necrosis of Rodent Tumors at 3.0T. Investigative Radiology, 2011, 46, 531-538.	6.2	11
141	Comparison of two vascular-disrupting agents at a clinically relevant dose in rodent liver tumors with multiparametric magnetic resonance imaging biomarkers. Anti-Cancer Drugs, 2012, 23, 12-21.	1.4	11
142	A safety study on single intravenous dose of tetrachloro-diphenyl glycoluril [iodogen] dissolved in dimethyl sulphoxide (DMSO). Xenobiotica, 2013, 43, 730-737.	1.1	11
143	Biodistribution and radiation dosimetry of radioiodinated hypericin as a cancer therapeutic. International Journal of Oncology, 2014, 44, 819-829.	3.3	11
144	Threeâ€dimensional contrasted visualization of pancreas in rats using clinical MRI and CT scanners. Contrast Media and Molecular Imaging, 2015, 10, 379-387.	0.8	11

#	Article	IF	CITATIONS
145	Biodistribution and anti-tumor efficacy of intratumorally injected necrosis-avid theranostic agent radioiodinated hypericin in rodent tumor models. Journal of Drug Targeting, 2015, 23, 371-379.	4.4	11
146	Synthesis and Evaluation of ¹³¹ I-Skyrin as a Necrosis Avid Agent for Potential Targeted Radionuclide Therapy of Solid Tumors. Molecular Pharmaceutics, 2016, 13, 180-189.	4.6	11
147	Visualization, Quantification and Characterization of Caerulein-Induced Acute Pancreatitis in Rats by 3.0T Clinical MRI, Biochemistry and Histomorphology. Theranostics, 2017, 7, 285-294.	10.0	11
148	Predicting Therapeutic Efficacy of Vascular Disrupting Agent CA4P in Rats with Liver Tumors by Hepatobiliary Contrast Agent Mn-DPDP-Enhanced MRI. Translational Oncology, 2020, 13, 92-101.	3.7	11
149	Electrodes and Multiple Electrode Systems for Radio Frequency Ablation: A Proposal for Updated Terminology. Advances in Experimental Medicine and Biology, 2006, 574, 57-73.	1.6	11
150	An overview of translational (radio)pharmaceutical research related to certain oncological and non-oncological applications. World Journal of Methodology, 2013, 3, 45.	3.5	11
151	Exploration of the mechanism underlying the tumor necrosis avidity of hypericin. Oncology Reports, 2008, , .	2.6	10
152	Improved clearance of radioiodinated hypericin as a targeted anticancer agent by using a duodenal drainage catheter in rats. Experimental Biology and Medicine, 2013, 238, 1437-1449.	2.4	10
153	Everolimus halts hepatic cystogenesis in a rodent model of polycystic-liver-disease. World Journal of Gastroenterology, 2017, 23, 5499.	3.3	10
154	Role of Contrast Agent Perfusion and of Diffusion in the NMR Signal Enhancement of Liver Lesions. Journal of Computer Assisted Tomography, 1992, 16, 690-698.	0.9	9
155	Radiolabeling and preliminary biological evaluation of a 99mTc(CO)3 labeled 3,3′-(benzylidene)-bis-(1H-indole-2-carbohydrazide) derivative as a potential SPECT tracer for in vivo visualization of necrosis. Bioorganic and Medicinal Chemistry Letters, 2011, 21, 502-505.	2.2	9
156	Exploring diagnostic potentials of radioiodinated sennidin A in rat model of reperfused myocardial infarction. International Journal of Pharmaceutics, 2015, 495, 31-40.	5.2	9
157	Vascular disrupting agent in pancreatic and hepatic tumour allografts: observations of location-dependent efficacy by MRI, microangiography and histomorphology. British Journal of Cancer, 2017, 117, 1529-1536.	6.4	9
158	Potentiation of Photodynamic Therapy with Hypericin by Mitomycin C in the Radiation-induced Fibrosarcoma–1 Mouse Tumor Model¶. Photochemistry and Photobiology, 2003, 78, 278.	2.5	9
159	Improved therapeutic outcomes of thermal ablation on rat orthotopic liver allograft sarcoma models by radioiodinated hypericin induced necrosis targeted radiotherapy. Oncotarget, 2016, 7, 51450-51461.	1.8	9
160	Incidence and prognosis of liver metastasis at diagnosis: a pan-cancer population-based study. American Journal of Cancer Research, 2020, 10, 1477-1517.	1.4	9
161	Manganese-Metalloporphyrin (ATN-10) as a Tumor-localizing Agent: Magnetic Resonance Imaging and Inductively Coupled Plasma Atomic Emission Spectroscopy Study with Experimental Brain Tumors. Neurosurgery, 1999, 44, 1146-1149.	1.1	8
162	Proper definitions of MRI contrast enhancement in liver tumors. Journal of Gastroenterology, 2010, 45, 349-350.	5.1	8

#	Article	IF	CITATIONS
163	Continuing pursuit for ideal systemic anticancer radiotherapeutics. Investigational New Drugs, 2012, 30, 2050-2065.	2.6	8
164	Synthesis and biological evaluation of 68Ga labeled bis-DOTA-3,3′-(benzylidene)-bis-(1H-indole-2-carbohydrazide) as a PET tracer for in vivo visualization of necrosis. Bioorganic and Medicinal Chemistry Letters, 2013, 23, 3216-3220.	2.2	8
165	Synthesis and biological evaluation of 68Ga-bis-DOTA-PA as a potential agent for positron emission tomography imaging of necrosis. Nuclear Medicine and Biology, 2013, 40, 816-822.	0.6	8
166	Trapping effect on a small molecular drug with vascular-disrupting agent CA4P in rodent H22 hepatic tumor model:in vivomagnetic resonance imaging and postmortem inductively coupled plasma atomic emission spectroscopy. Journal of Drug Targeting, 2015, 23, 436-443.	4.4	8
167	Experimental evaluation of radioiodinated sennoside B as a necrosis-avid tracer agent. Journal of Drug Targeting, 2015, 23, 180-190.	4.4	8
168	Effects of Glycosylation on Biodistribution and Imaging Quality of Necrotic Myocardium of Iodine-131-Labeled Sennidins. Molecular Imaging and Biology, 2016, 18, 877-886.	2.6	8
169	Molecular imaging of myocardial necrosis: an updated mini-review. Journal of Drug Targeting, 2020, 28, 565-573.	4.4	8
170	An overview on development and application of an experimental platform for quantitative cardiac imaging research in rabbit models of myocardial infarction. Quantitative Imaging in Medicine and Surgery, 2014, 4, 358-75.	2.0	8
171	A Model In Vitro Study Using Hypericin: Tumor-Versus Necrosis-Targeting Property and Possible Mechanisms. Biology, 2020, 9, 13.	2.8	7
172	Predicting Clinical Efficacy of Vascular Disrupting Agents in Rodent Models of Primary and Secondary Liver Cancers: An Overview with Imaging-Histopathology Correlation. Diagnostics, 2020, 10, 78.	2.6	7
173	Abstract 1767: Oncocidia: a small molecule dual targeting pan-anticancer theragnostic strategy. Cancer Research, 2014, 74, 1767-1767.	0.9	7
174	Micro-HCCs in rats with liver cirrhosis: paradoxical targeting effects with vascular disrupting agent CA4P. Oncotarget, 2017, 8, 55204-55215.	1.8	7
175	Targetability and Biodistribution of Radioiodinated Hypericin: Comparison between Microdosing and Carrier-Added Preparations. Anti-Cancer Agents in Medicinal Chemistry, 2014, 14, 852-861.	1.7	7
176	Intra-individual comparison of therapeutic responses to vascular disrupting agent CA4P between rodent primary and secondary liver cancers. World Journal of Gastroenterology, 2018, 24, 2710-2721.	3.3	7
177	Synthesis and preliminary biological evaluation of a99mTc-labeled hypericin derivative as a necrosis avid imaging agent. Journal of Labelled Compounds and Radiopharmaceuticals, 2008, 51, 33-40.	1.0	6
178	A Canine Model of Proximal Descending Thoracic Aortic Aneurysm Created with an Autologous Pericardial Patch. Annals of Thoracic and Cardiovascular Surgery, 2013, 19, 131-135.	0.8	6
179	Differentiation between Malignant and Benign Solitary Lesions in the Liver with ¹⁸ FDG PET/CT: Accuracy of Age-related Diagnostic Standard. Journal of Cancer, 2015, 6, 40-47.	2.5	6

180 Intravitreally Injected Fluid Dispersion: Importance of Injection Technique. , 2017, 58, 1434.

6

#	Article	IF	CITATIONS
181	Pancreatic imaging: Current status of clinical practices and small animal studies. World Journal of Methodology, 2017, 7, 101-107.	3.5	6
182	Rheinâ€based necrosisâ€avid MRI contrast agents for early evaluation of tumor response to microwave ablation therapy. Magnetic Resonance in Medicine, 2019, 82, 2212-2224.	3.0	6
183	Discovery of necrosis avidity of rhein and its applications in necrosis imaging. Journal of Drug Targeting, 2020, 28, 904-912.	4.4	6
184	Differentiation of Residual Tumor from Benign Periablational Tissues after Radiofrequency Ablation: The Role of MR Imaging Contrast Agents. Radiology, 2005, 237, 745-749.	7.3	5
185	ls There a Decline in the Vascular Event Rate after Transient Ischemic Attack or Stroke in Antiplatelet Trials?. Cerebrovascular Diseases, 2009, 28, 439-447.	1.7	5
186	Multimodality Imaging of Endothelial Progenitor Cells with a Novel Multifunctional Probe Featuring Positive Magnetic Resonance Contrast and Near-Infrared Fluorescence. Molecular Imaging, 2011, 10, 7290.2010.00055.	1.4	5
187	MR Contrast Agents for Cardiac Imaging. Medical Radiology, 2011, , 31-51.	0.1	5
188	Study on the Microbial Safety of an Infusion Set for Contrast-Enhanced Imaging. Investigative Radiology, 2012, 47, 247-251.	6.2	5
189	Cerebral alveolar echinococcosis: A report of two cases. Clinical Neurology and Neurosurgery, 2012, 114, 717-720.	1.4	5
190	Effects of skeleton structure on necrosis targeting and clearance properties of radioiodinated dianthrones. Journal of Drug Targeting, 2016, 24, 566-577.	4.4	5
191	A methodology for constraining power in finite element modeling of radiofrequency ablation. International Journal for Numerical Methods in Biomedical Engineering, 2017, 33, e2834.	2.1	5
192	Evaluation of Radioiodinated 1,4-Naphthoquinones as Necrosis Avid Agents for Rapid Myocardium Necrosis Imaging. Molecular Imaging and Biology, 2018, 20, 74-84.	2.6	5
193	First Evaluation of Radioiodinated Flavonoids as Necrosis-Avid Agents and Application in Early Assessment of Tumor Necrosis. Molecular Pharmaceutics, 2018, 15, 207-215.	4.6	5
194	A piecewise function of resistivity of liver: determining parameters with finite element analysis of radiofrequency ablation. Medical and Biological Engineering and Computing, 2018, 56, 385-394.	2.8	5
195	Pictorial Imaging-Histopathology Correlation in a Rabbit with Hepatic VX2 Tumor Treated by Transarterial Vascular Disrupting Agent Administration. International Journal of Medical Sciences, 2020, 17, 2269-2275.	2.5	5
196	Radiofrequency ablation with four electrodes as a building block for matrix radiofrequency ablation: Ex vivo liver experiments and finite element method modelling. Influence of electric and activation mode on coagulation size and geometry. Surgical Oncology, 2020, 33, 145-157.	1.6	5
197	Preparation and validation of cyclodextrin-based excipients for radioiodinated hypericin applied in a targeted cancer radiotherapy. International Journal of Pharmaceutics, 2021, 599, 120393.	5.2	5
198	Monitoring reperfused myocardial infarction with delayed left ventricular systolic dysfunction in rabbits by longitudinal imaging. Quantitative Imaging in Medicine and Surgery, 2018, 8, 754-769.	2.0	5

#	Article	IF	CITATIONS
199	Bifunctional staining for <i>ex vivo</i> determination of area at risk in rabbits with reperfused myocardial infarction. World Journal of Methodology, 2013, 3, 27.	3.5	5
200	Cancer Models—Multiparametric Applications of Clinical MRI in Rodent Hepatic Tumor Model. Methods in Molecular Biology, 2011, 771, 489-507.	0.9	4
201	Proper Handling of Research with Invalid Conclusions [letter]. Radiology, 2003, 229, 608-610.	7.3	3
202	Animal models of ischemic heart disease for in vivo cardiac MR imaging research. International Journal of Modelling, Identification and Control, 2010, 9, 288.	0.2	3
203	Biliary and duodenal drainage for reducing the radiotoxic risk of antineoplastic ¹³¹ I-hypericin in rat models. Experimental Biology and Medicine, 2015, 240, 1764-1773.	2.4	3
204	Evaluation of Necrosis Avidity and Potential for Rapid Imaging of Necrotic Myocardium of Radioiodinated Hypocrellins. Molecular Imaging and Biology, 2018, 20, 551-561.	2.6	3
205	Synthesis and Evaluation of Diindole-Based MRI Contrast Agent for In Vivo Visualization of Necrosis. Molecular Imaging and Biology, 2020, 22, 593-601.	2.6	3
206	Re: "Endovascular Aneurysm Sealing for the Treatment of Ruptured Abdominal Aortic Aneurysms― Journal of Endovascular Therapy, 2015, 22, 956-957.	1.5	2
207	Excretion and toxicity evaluation of ¹³¹ I-Sennoside A as a necrosis-avid agent. Xenobiotica, 2017, 47, 980-988.	1.1	2
208	Hypothesis: What is the Best We Can Do with Hydroxychloroquine for COVID-19?. Clinical Epidemiology, 2020, Volume 12, 1139-1144.	3.0	2
209	Untiring Pursuit for Glucarate-Based Molecular Imaging Probes. Molecular Imaging and Biology, 2021, 23, 310-322.	2.6	2
210	Design and Evaluation of Rhein-Based MRI Contrast Agents for Visualization of Tumor Necrosis Induced by Combretastatin A-4 Disodium Phosphate. Molecular Imaging and Biology, 2021, 23, 220-229.	2.6	2
211	Rat model of cholelithiasis with human gallstones implanted in cholestasis-induced virtual gallbladder. World Journal of Methodology, 2016, 6, 154.	3.5	2
212	Development and characterization of a rat brain metastatic tumor model by multiparametric magnetic resonance imaging and histomorphology. Clinical and Experimental Metastasis, 2022, , 1.	3.3	2
213	Heterogeneity of Synchronous Lung Metastasis Calls for Risk Stratification and Prognostic Classification: Evidence from a Population-Based Database. Cancers, 2022, 14, 1608.	3.7	2
214	Development and characterization of a chick embryo chorioallantoic membrane (CAM) based platform for evaluation of vasoactive medications. Microvascular Research, 2022, 142, 104372.	2.5	2
215	Radiofrequency Ablation: The Use of Appropriate Terms and the Citation of Prior Art. Academic Radiology, 2006, 13, 1047-1048.	2.5	1
216	Potentiation of Photodynamic Therapy with Hypericin by Mitomycin C in the Radiation-induced Fibrosarcoma-1 Mouse Tumor Model A¶. Photochemistry and Photobiology, 2007, 78, 278-282.	2.5	1

#	Article	IF	CITATIONS
217	A Place for Radiofrequency Ablation in the Treatment of Resectable Colorectal Liver Metastases?. Annals of Surgical Oncology, 2008, 15, 2064-2065.	1.5	1
218	Development, evaluation and application of reperfused liver infarction in rats as a practical model for studying ischemic diseases and screening new drugs. International Journal of Modelling, Identification and Control, 2010, 9, 247.	0.2	1
219	Evaluation of a metalloporphyrin (THPPMnCl) for necrosis-affinity in rat models of necrosis. Journal of Drug Targeting, 2015, 23, 926-935.	4.4	1
220	PD806. Anti-Cancer Drugs, 2015, 26, 148-159.	1.4	1
221	A multifunctional contrast dye for morphological research. Microscopy Research and Technique, 2016, 79, 111-121.	2.2	1
222	An Imaging and Histological Study on Intrahepatic Microvascular Passage of Contrast Materials in Rat Liver. BioMed Research International, 2017, 2017, 1-11.	1.9	1
223	Evaluation of necrosis avidity of radioiodinated 5-hydroxytryptophan and its potential applications in myocardial infarction imaging. Chinese Chemical Letters, 2019, 30, 83-86.	9.0	1
224	What is the purpose of launching the <i>World Journal of Methodology</i> ?. World Journal of Methodology, 2011, 1, 1.	3.5	1
225	Radioiodinated hypericin as a tracer for detection of acute myocardial infarction: SPECT-CT imaging in a swine model. Journal of Nuclear Cardiology, 2022, 29, 3432-3439.	2.1	1
226	Magnetic resonance imaging of experimental tracheal transplantation. Academic Radiology, 1996, 3, 154-158.	2.5	0
227	Contrast Agents for Cardiac MRI. , 2005, , 33-50.		0
228	Rodent models and magnetic resonance imaging: diagnostic and therapeutic utilities for stroke. International Journal of Modelling, Identification and Control, 2010, 9, 275.	0.2	0
229	Choices for animal models of atherosclerosis in MR molecular imaging study. International Journal of Modelling, Identification and Control, 2010, 9, 318.	0.2	0
230	Magnetic Resonance Imaging of Cancer Therapy. , 2014, , 95-126.		0
231	A newly found handbook for developing vaccines during World War II in China: the legacy of global responses to crises. Emerging Microbes and Infections, 2020, 9, 1997-1999.	6.5	0
232	Editorial for "Tumor Stiffness Measurements on Magnetic Resonance Elastography for Single Nodular Hepatocellular Carcinomas Can Predict Tumor Recurrence after Hepatic Resection". Journal of Magnetic Resonance Imaging, 2021, 53, 597-598.	3.4	0
233	Characterization of Liver Tumors with Hepatobiliary Contrast Agent Enhanced Magnetic Resonance Imaging. , 1996, , 11-24.		0
234	Have we lost an essential link between coordination chemistry and medical applications?. Coordination Chemistry Reviews, 2022, 460, 214465.	18.8	0